Genetic rescue of mitochondrial and skeletal muscle impairment in an iPSC model of coenzyme Q10 deficiency

Romero-Moya D[1], Santos-Ocaña C [2,3], Castaño J [1], Garrabou G [3,4], Rodríguez-Gómez JA [5], Ruiz-Bonilla V [6,7], Bueno C [1], González-Rodríguez P [5,6], Giorgetti A [1], Perdiguero E [6,7], Prieto C [1], Moren-Nuñez C [3,4], Fernández-Ayala DJ [2,3], Victoria Cascajo M [2,3], Velasco I [8,9], Canals JM6,10,11,12, Montero R3,13, Yubero D [13], Jou C3,13, López-Barneo J [5,6], Cardellach F [3,4], Muñoz-Cánoves P [6,7,14,15], Artuch R [3,13], Navas P [2,3], Menendez P [1,14,16].

[1] Josep Carreras Leukemia Research Institute, Department of Biomedical Sciences, Faculty of Medicine and Health Sciences, University of Barcelona, Barcelona, Spain.[2] Centro Andaluz de Biología del Desarrollo, Universidad Pablo Olavide-CSIC, Sevilla, Spain.[3] CIBER de Enfermedades Raras (CIBERER), Spain.[4] Muscle Research and Mitochondrial Function Laboratory, Cellex-IDIBAPS-Faculty of Medicine and Health Sciences, University of Barcelona, Barcelona, Spain.[5] Institute of Biomedicine of Seville, Hospital Universitario Virgen del Rocío-Consejo Superior de Investigaciones Científicas (CSIC)-University of Seville, Seville, Spain.[6] CIBER on Neurodegenerative Diseases (CIBERNED), Barcelona, Spain.[7] Pompeu Fabra University (UPF), Barcelona, Spain. [8] Insituto de Fisiología Celular-Neurociencias, Universidad Nacional Autónoma de México, México. [9] Laboratorio de Reprogramación Celular del IFC en el Instituto Nacional de Neurología y Neurocirugía "Manuel Velasco Suárez", México DF, México. [10] Stem Cells and Regenerative Medicine Laboratory, Production and validation center of advanced therapies (Creatio) Department of Biomedical Sciences, Faculty of Medicine and Health Sciences, University of Barcelona, Barcelona, Spain. [11] Neuroscience Institute, University of Barcelona, Barcelona, Spain. [12] August Pi i Sunyer Biomedical Research Institute (IDIBAPS), Barcelona, Spain. [13] Clinical Biochemistry Department, Pediatric Research Institute-Hospital Sant Joan de Déu, Barcelona, Spain. [14] Institució Catalana Recerca Estudis Avančats (ICREA), Lluís Companys 23, Barcelona, Spain.[15] Spanish National Center on Cardiovascular Research (CNIC), Madrid, Spain. [16] Centro de Investigación Biomédica en Red de Cáncer (CIBERONC), ISCIII, Spain.

Running Title: iPSC and Coenzyme Q10

Key words: Coenzyme Q10, COQ4, iPSC, CRISPR-Cas9, dopaminergic & motor neurons, skeletal muscle.

*__Correspondence should be addressed to:__
Pablo Menendez PhD. ICREA Research Professor
Josep Carreras Leukemia Research Institute. School of Medicine. University of Barcelona.
Casanova 143, 08036. Barcelona. Spain. pmenendez@carrerasresearch.org

ABSTRACT

Coenzyme Q_{10} (CoQ_{10}) plays a crucial role in mitochondria as an electron carrier within the mitochondrial respiratory chain (MRC), and is an essential antioxidant. Mutations in genes responsible for CoQ_{10} biosynthesis (*COQ* genes) cause primary CoQ_{10} deficiency, which is a rare and heterogeneous mitochondrial disorder with no clear genotype-phenotype association, mainly affecting tissues with high-energy demand including brain and skeletal muscle (SkM). Here, we report a 4-year old girl diagnosed with modest mental retardation and lethal rhabdomyolysis harboring a heterozygous mutation (c.483G>C (E161D)) in *COQ4*. The patient's fibroblasts showed a severe decrease in [CoQ_{10}], CoQ_{10} biosynthesis and MRC activity affecting complexes I/II+III. *Bona fide* iPSC carrying the *COQ4* mutation (CQ4-iPSC) were generated, characterized and genetically edited using the CRISPR-Cas9 system ($CQ4^{ed}$-iPSC). Extensive differentiation and metabolic assays of control-iPSC, CQ4-iPSC and $CQ4^{ed}$-iPSC demonstrated a genotype-phenotype association, faithfully reproducing the disease features. Similar to the patient`s symptoms, the *COQ4* mutation in iPSC was associated with CoQ_{10} deficiency, metabolic dysfunction and impaired differentiation into SkM; however, it did not impair iPSC differentiation into dopaminergic or motor neurons. This study offers an unprecedented iPSC model recapitulating CoQ_{10} deficiency-associated functional and metabolic phenotypes caused by *COQ4* mutation.

Coenzyme Q_{10} (CoQ_{10}) is a lipid-soluble molecule ubiquitous to cellular membranes that has essential functions in many cellular processes including energy/ATP production, where it shuttles electrons from complex I and II to complex III in the mitochondrial respiratory chain (MRC). CoQ_{10} also participates in beta-oxidation of fatty acids, pyrimidine biosynthesis, and it is one of the main cellular antioxidants[1, 2]. Several proteins are encoded by different *COQ* genes and are involved in the pathway of CoQ_{10} biosynthesis between the cytoplasm and mitochondria by functioning as a multienzymatic complex[3]. Several mutations in genes involved in CoQ_{10} biosynthesis, such as *COQ2*[4-7], *COQ6*[8], *ADCK3*[7, 9, 10], *ADCK4*[11], *COQ9*[7, 12], *PDSS1*[13], *PDSS2*[7, 14] and *COQ7*[15], have been described, and all result in a reduction in CoQ_{10} levels. CoQ_{10} levels below 50% of standard values are indicative of CoQ_{10} deficiency, which is a rare and heterogeneous group of metabolic/mitochondrial disorders (OMIM#607426)[16] frequently diagnosed during childhood. CoQ_{10} deficiency associates with multiple clinical phenotypes including kidney failure[13] and neuromuscular diseases, such as mental retardation, seizures, and ataxias, affecting tissues with high energetic demand such as muscle and neurons[16-18].

It has been suggested that COQ4 has an essential structural and functional role for the biosynthesis of CoQ_{10}[19-21]. Indeed, *COQ4* mutations as well as *COQ4* haploinsufficiency cause a broad spectrum of mitochondrial disorders associated with CoQ_{10} deficiency[22, 23]. We diagnosed CoQ_{10} deficiency in a 4-year-old girl with a heterozygous mutation (c.483 G>C) in *COQ4*. This patient did not display (or very mild) symptoms of impaired neurodevelopment or neurodegeneration, but presented severe metabolic/mitochondrial defects accompanied with lethal rhabdomyolysis. CoQ_{10} deficiency is a heterogeneous disease, and a major obstacle to study this disorder is the lack of association between the genotype and phenotype[3, 24], which partly explains the highly variable patient response to CoQ_{10} supplementation[3, 25, 26].

Human disease is generally studied once all (epi)genetic/metabolic insults have already occurred and, therefore, the mechanisms by which disease-specific mutations impair normal homeostasis are not amenable to analysis with patient samples. In this regard, induced pluripotent stem cells (iPSC) together with genome editing strategies for correction of disease-causing mutations are powerful tools for modeling different aspects of human disease that cannot otherwise be addressed by patient sample analyses or animal models[27, 28]. iPSC are routinely generated from different cell types derived from both healthy donors and patients[29-32], thus providing a unique *in vitro* platform to explore the developmental impact of disease-specific genetic aberrations on human stem cell fate, especially in early-onset or developmental diseases[27].

Here, we have generated and CRISPR/Cas9 edited iPSC from a patient carrying a *COQ4* mutation to model CoQ_{10} deficiency by analyzing the metabolic/mitochondrial status. Developmental and metabolic assays established a genotype-phenotype association. In line with the patient`s symptoms, the *COQ4* mutation was associated with CoQ_{10} deficiency, metabolic dysfunction and impaired differentiation into skeletal muscle (SkM); however, the *COQ4* mutation did not impair iPSC differentiation into neural tissues. This study offers a unique human iPSC model recapitulating CoQ_{10} deficiency-associated functional and metabolic phenotypes caused by *COQ4* mutation.

RESULTS

COQ4 mutation causes a mitochondrial disorder associated with CoQ_{10} deficiency

A 4-year-old girl was diagnosed in our Institution with modest mental retardation and lethal rhabdomyolysis. Genetic analysis identified a heterozygous c.483 G>C mutation in the *COQ4*, leading to the amino acid change E161D **(Fig 1A)**. *COQ4* mutations have been reported to be responsible for early-onset mitochondrial diseases with heterogeneous clinical presentations and associated CoQ_{10} deficiency. Analysis of fibroblasts revealed that the concentration and biosynthesis of CoQ_{10} was 75% and 87% lower, respectively, in CQ4-F

than in Ctrl-F **(Fig 1B, C)**. The expression of key *COQ* genes involved in CoQ_{10} biosynthesis was appreciably higher in CQ4-F than in Ctrl-F, suggestive of a transcriptional compensatory mechanism **(Fig. 1D)**. In line with its role in electron transport, the reduction in CoQ_{10} in CQ4-F was reflected in the functional reduction of 41% and 64% in the activity of complex I+III and II+III, respectively **(Fig 1E)**. CoQ_{10} is involved in pyrimidine biosynthesis, which is a requirement for cell proliferation[2, 5, 7]. Accordingly, cell proliferation was considerably lower in CQ4-F than in Ctrl-F **(Fig 1F)**. Moreover, the proportion of cycling cells was significantly lower for CQ4-F than for Ctrl-F (33% vs 24%; p=0.09, **Fig 1G**), and this was accompanied by a significant (17-fold) increase in senescence as measured by SA-β-Gal staining, and a 2-fold increase in the level of the senescence-associated gene *p16* (*CDKN2A*, **Fig 1H**). Conversely, the level of apoptosis was not different between CQ4-F and Ctrl-F **(Fig 1I)**. Histological analysis of the patient's SkM revealed extensive damage associated with rhabdomyolysis **(Fig 1J)**, as shown by disorganized tissue structure and loss of expression of the mitochondrial markers SDH and COX **(Fig 1J)**.

Generation and characterization of CQ4-iPSCs.

CQ4-F were reprogrammed in an attempt to model CoQ_{10} deficiency by exploring the functional impact of *COQ4* mutation on human pluripotent stem cell fate. Patient and control fibroblasts were transduced with OSKM-expressing Sendai virus (SeV) following the experimental design outlined in **Fig 2A**. iPSC colonies emerged 16–18 days after OSKM transduction and were picked for further characterization (**Fig 2A**). Reprogramming efficiency was ~5-fold higher in Ctrl-F than in CQ4-F (0.8% vs 0.17%, **Fig 2B**), likely reflecting the impaired proliferation capacity of CQ4-F. PCR analysis and Sanger sequencing confirmed the c.483 G>C mutation in all CQ4-iPSC clones **(Fig 2C).** After 8–10 passages, iPSCs were OSKM transgene independent as revealed by immunostaining and qRT-PCR analysis for SeV **(Fig 2D)**. Characterization of iPSC revealed an embryonic stem cell (ESC)-like morphology and positive alkaline phosphatase staining **(Fig S1A)**. In addition, the pluripotency-associated genes *OCT4*, *SOX2*, *REX1*, *NANOG* and *CRIPTO* were

expressed at comparable levels to human ESC **(Fig S1B)**. Similarly, immunocytological staining revealed *bona fide* expression of OCT4, NANOG, TRA-1-60 and SSEA4 in both CQ4- and Ctrl-iPSC **(Fig S1C)**. Endogenous expression of *NANOG* and *OCT4* was accompanied by the extensive loss of CpG methylation in their promoters **(Fig S1D)**. Both Ctrl- and CQ4-iPSC consistently displayed a diploid karyotype after >20 passages **(Fig S1E)**, and formed teratomas in immunodeficient mice comprising tissue representing all three germ layers **(Fig S1F)**.

iPSC gene edition by CRISPR/Cas9 system.

Because the differentiation capacity among iPSC lines is influenced by (epi)genetic variability[33, 34], the optimal scenario to unravel genotype-phenotype associations is to use isogenic iPSC lines. We therefore used the CRISPR/Cas9 system to gene edit CQ4-iPSCs (CQ4^{ed}-iPSC). From the four sgRNAs designed surrounding the c.483 G>C mutation in exon 5 of the *COQ4* allele, one sgRNA was found to have a high cleavage activity (~25%, data not shown) in the T7 surveyor assay, cutting 8 nucleotides upstream of the mutation. Next, we designed a 90 bp-long donor ssDNA carrying a silent mutation for the generation of a Taqα1 restriction site and the mutation corrected codon **(Fig 2E)**. CQ4-iPSCs were co-transfected with Cas9-GFP vector and ssDNA and, 2 days later, GFP+ clones were FACS-sorted as single cells. All individual GFP$^+$ established clones were analyzed by PCR and restriction fragment length polymorphism, obtaining an allele digestion where the editing was performed **(Fig 2F)**. Homozygous editing of the COQ4 mutation was observed in several clones, which was further confirmed by sequencing **(Fig 2F,G)**. The top off-target predicted beforehand, *GRID2,* was sequenced in CQ4^{ed}-iPSCs and was consistently found to be germline configuration, demonstrating the specificity of the sgRNA/gDNA used to edit the *COQ4* mutation **(Fig 2H)**. Importantly, CQ4^{ed}-iPSC remained pluripotent, as shown by expression of pluripotency-associated transcription factors **(Fig 2I)** and surface markers **(Fig S1G)**, and was cytogenetically stable **(Fig S1H)**.

COQ4 genome edition reverses metabolic/mitochondrial dysfuction

CoQ_{10} is a lipophilic molecule involved in the MRC[1, 2], and low levels of CoQ_{10} in fibroblasts or muscle biopsies are linked to CoQ_{10} deficiency[16]. To obtain a reference value for CoQ_{10}, we measured its concentration in different pluripotent stem cells (hESC and hiPSC) **(Fig 3A left)**. CoQ_{10} concentration and biosynthesis was significantly lower (36% and 61%, respectively) in CQ4-iPSCs than in Ctrl-iPSC and hESC **(Fig 3A right, 3B)**. Strikingly, a full restoration both of CoQ_{10} concentration (25% increase) and biosynthesis (50% increase) was found in $CQ4^{ed}$-iPSC **(Fig 3C,D)**. Similarly, the activity of MRC complexes I+III and II+III was recovered in the $CQ4^{ed}$-iPSC (~50% increase) **(Fig 3E)**. We next evaluated oxidative phosphorylation and glycolysis by ATP quantification, basal live-cell oxygen consumption rate (OCR) and extracellular acidification rate (ECAR). To produce the same ATP concentration **(Fig 3F)**, CQ4-iPSC ECAR **(Fig 3G)** and OCR **(Fig 3H)** rates were 2-fold higher than in $CQ4^{ed}$-iPSC, suggesting a respiration dysfunction as confirmed by a 2-fold higher proton leak (difference between oligomycin- and antinomycin A-mediated inhibition of OCRs) in the mutated relative to edited iPSC **(Fig 3I).** Together, these results show that CQ4-iPSC maintain the CoQ_{10} deficiency and metabolic dysfunction found in CQ4-F, which is fully reversed upon correction of the *COQ4* mutation, thus directly linking c.483 G>C *COQ4* with the dysfunctional metabolic phenotype.

COQ4 mutation does not impair iPSC differentiation into dopaminergic or motor neurons

The majority of CoQ_{10}-deficient patients present with neurological symptoms[17, 18]. Importantly, however, the patient here described did not have neurological deficits other than a modest mental retardation. Whether and how *COQ* mutations influence neurodevelopment remains obscure. To study the potential developmental impact of the *COQ4* mutation in human neurogenesis, Ctrl-, CQ4- and $CQ4^{ed}$-iPSC were differentiated into dopaminergic (DA) neurons and motor neurons (MN) using well-established protocols **(Fig 4A, 5A)**[35, 36]. Successful differentiation was confirmed by flow cytometry as demonstrated by a progressive increase in the

proportion of NCAM$^+$ cells, with >80% (DA) and >60% (MN) of NCAM$^+$ cells formed by day 30 of differentiation irrespective of the iPSC genotype (**Fig 4B, 5B**). We then evaluated the differentiation output of neural progenitors (SOX2$^+$NESTIN$^+$) and immature neurons (TUJ1$^+$) by confocal imaging at early time points (day 15–20 of neural induction). No differences were found between Ctrl- and CQ4-iPSCs for differentiation into neural progenitors (~50% and ~35–50% SOX2$^+$NESTIN$^+$ cells under DA and MN differentiation conditions, respectively) or total neurons (~15 and ~22% TUJ1$^+$ cells under DA and MN differentiation conditions, respectively) (**Fig 4C, 5C**). Similarly, at later time points (~day 30–40 of differentiation), the proportion of TUJ1$^+$ differentiating neurons between Ctrl- and CQ4-iPSCs was very similar (~30–40%) regardless of the differentiation protocol (**Fig 4D, 5D**). Furthermore, the yield of TUJ1$^+$TH$^+$ DA (~8%) and TUJ1$^+$HB9$^+$/TUJ1$^+$ISL1$^+$ MN (~4%) was also similar between Ctrl- and CQ4-iPSCs (**Fig 4D, 5D**). Accordingly, CQ4^{ed}-iPSC differentiated into DA (**Fig 4C, D**) and MN (**Fig 5C, D**) neurons as well as neural precursors to a similar extent to that achieved by CQ4-iPSC. Immunofluorescence-based quantification was confirmed by qRT-PCR expression analysis of DA-specific (*FOXA2* and *TH*, **Fig 4E**) and MN-specific (*LHX3* and *FOXP1*, **Fig 5E**) master genes. We then carried out functional analyses to confirm these results. HPLC determination of dopamine release revealed very similar levels of dopamine in Ctrl- and CQ4-iPSC-derived neurons **(Fig 4F).** Whole patch clamp recording of MN (identified using the HB9-GFP reporter)[36, 37] indicated that CQ4-iPSC-derived MN were eletrophysiologically active with functional synapses after 40–50 days in culture. Moreover, CQ4-iPSC-derived MN displayed inward and outward currents, induced action potential and spontaneous firing similar to that found in neurons derived from Ctrl-iPSC **(Fig 5F)**[37, 38]**.** The comparable yields of DA and MN generated from Ctrl-, CQ4- and CQ4^{ed}-iPSCs may be explained by similar neural specification from genotypically distinct iPSCs as no differences were found for cell death (**Fig 4G, 5G**) or cell cycle/proliferative status (**Fig 4H, 5H**) of the emerging NCAM+ neurons. Of note, DA neurons from CQ4-iPSCs cycled slightly less that those from Ctrl- or CQ4^{ed}-iPSCs, possibly reflecting a role for *COQ4* in the cell

cycle of DA neurons. Together, these data reveal that the c.483 G>C mutation in *COQ4* does not impact DA or MN neurogenesis from iPSCs, recapitulating the patient's phenotype.

COQ4 mutation recapitulates the CoQ_{10}-deficiency-associated skeletal muscle functional and metabolic defects

Muscle impairment is common in CoQ_{10}-deficient patients[19], but it was especially life-threating in the patient reported here, who suffered from lethal rhabdomyolysis that was clinically unmanageable, resulting in her death from fatal kidney damage as a result of myoglobinuria. To study the developmental and metabolic impact of the *COQ4* mutation in skeletal myogenesis, Ctrl-, CQ4- and $CQ4^{ed}$-iPSC were differentiated into SkM following a well-established protocol developed in the Perlingeiro laboratory [32]. Transgenic Ctrl-, CQ4- and $CQ4^{ed}$-iPSC carrying a PAX7-GFP-expressing inducible lentivector were generated, and myogenic specification was induced as described in **Fig 6A**. PAX7-GFP-expressing myogenic progenitors were GFP FACS-purified on day 15 of myogenic development **(Fig 6A,B)**. All FACS-sorted GFP^+ cells co-expressed PAX7, demonstrating the reliability of the inducible reporter **(Fig 6C).** Although the cell cycle profile (**Fig 6D**) and the level of apoptosis (**Fig 6E)** was very similar between CQ4- and Ctrl-$PAX7^+$ myogenic progenitors, the number of senescent CQ4-$PAX7^+$ cells was 2-fold higher, a phenotype that was corrected in $CQ4^{ed}$-$PAX7^+$ myogenic progenitors **(Fig 6F)**. The enhanced senescence observed in CQ4-$PAX7^+$ myogenic progenitors might be explained by their increased ROS production (**Fig 6G**) leading to a 1-log reduction in cell expansion (**Fig 6H**); both of these functional properties were corrected in $CQ4^{ed}$-$PAX7^+$ myogenic progenitors (**Fig 6G,H**).

$PAX7^+$ myogenic progenitors were allowed to further mature into myocytes/myotubes as detailed in **Fig 6A**[32]. Consistent with the muscle damage observed in the CQ4-mutated patient, CQ4-$PAX7^+$ myogenic progenitors displayed a significant maturation impairment as revealed by a 30% reduction in the generation of mature

MYH1+ cells (**Fig 6I**) and a 3-fold reduction in the expression of creatine kinase (CK) (**Fig 6J**), a master enzyme expressed in SkM that ensures an energy reservoir for the rapid buffering and regeneration of ATP. Importantly, both the generation of MYH1+ cells and the levels of CK were at control levels in myocytes/myotubes derived from CQ4ed-PAX7+ myogenic progenitors (**Fig 6I,J**). In addition, gene expression analysis of the specific myogenic markers, myogenic regulatory factor *MYF5*, myogenin (*MGN*) and myosin heavy chain 3 (*MYH3*), showed that their kinetics of expression were deregulated in CQ4-PAX7+ as compared with Ctrl-PAX7+ differentiating myocytes/myotubes (**Fig 6K**); however, their expression kinetics returned to control values in CQ4ed-PAX7+ differentiating myocytes/myotubes (**Fig 6K**).

Finally, we analyzed the metabolic impact of the *COQ4* mutation in SkM derivatives generated from Ctrl-, CQ4- and CQ4ed-PAX7+ myogenic progenitors. Consistent with the patient's phenotype, morphometric image analysis of myocytes stained with TOM20 revealed abnormalities in mitochondrial morphology caused by the *COQ4* mutation (**Fig 6L**). Accordingly, CQ4-PAX7+ iPSC-derived myocytes/myotubes had smaller (nº mitochondria/cellular area, **Fig 6L-panel i**), more circular (**Fig 6L-panel ii**), less branched (FF, **Fig 6L-panel iii**), and shorter (mitochondrial length, **Fig 6L-panel iv**) mitochondria than Ctrl-PAX7+ iPSC-derived myocytes/myotubes[39]. Importantly, these mitochondrial dynamics-associated parameters were restored in CQ4ed-PAX7+ iPSC-derived myocytes/myotubes. In addition, MRC complex I+III activity was 50% lower in CQ4-PAX7+ iPSC-derived myocytes/myotubes than in Ctrl-PAX7+ counterparts, and this was fully restored in CQ4ed-PAX7+ iPSC-derived myocytes/myotubes, (**Fig 6M**). Collectively, these results establish the utility of an iPSC-based disease model to study genotype-phenotype associations, wherein the *COQ4* mutation faithfully reproduces the disease-associated SkM functional and metabolic defects.

DISCUSSION

CoQ_{10} deficiency comprises a growing number of metabolic disorders with neurological and extraneurological manifestation. Despite being considered a rare disease, next-generation DNA sequencing techniques coupled with well-established biochemical determination of CoQ_{10} biosynthesis has allowed the identification of a variety of primary and secondary CoQ_{10} deficiencies[40]. Primary deficiency of CoQ_{10} is an autosomal syndrome originating from mutations in genes responsible for CoQ_{10} biosynthesis. The pathogenesis of secondary CoQ_{10} deficiency is less studied but may be linked to assembly defects in oxidative phosphorylation (OxPhos) complexes/metabolic pathways[19, 41]. CoQ_{10} deficiency impairs OxPhos and global metabolic homeostasis, ultimately causing clinically heterogeneous mitochondrial diseases in primarily skeletal muscle and central nervous system, likely because the disruption of energy metabolism strongly affects tissues with high-energy demand[8, 42].

CoQ_{10} biosynthesis relies on a pathway involving at least 15 *COQ* and regulatory genes, and is carried out by a putative multi-subunit enzyme complex[3]. To date, mutations in numerous *COQ* genes involved in CoQ_{10} biosynthesis have been identified as the primary cause of CoQ_{10} deficiency, making the molecular diagnosis and clinical characterization challenging. However, there is not yet a clear association described between genotype and phenotype; mutations in different *COQ* genes may exert the same clinical phenotype or, *vice versa*, the same mutation in a specific *COQ* gene may confer distinct clinical manifestations[43]. The only currently available therapeutic approach for patients with CoQ_{10} deficiency is CoQ_{10} supplementation[44]. However, this is only partially successful perhaps due to the lack of association between *COQ* genotypes and clinical phenotype, and thus its effectiveness is questioned[4, 12, 45].

It has been recently suggested that COQ4 has an essential structural and functional role for the biosynthesis of CoQ_{10}, and *COQ4* mutations as well as *COQ4* haploinsufficiency cause a broad spectrum of mitochondrial disorders associated with CoQ_{10} deficiency[19-23, 46]. Here, we report a 4-year-old girl with a heterozygous c.483 G>C mutation in *COQ4* who displayed severe metabolic/mitochondrial deficits, extensive muscle damage

and lethal rhabdomyolysis. The *COQ4* mutation was associated with CoQ_{10} deficiency and MRC dysfunction, in line with the critical role of CoQ_{10} as an electron shuttle. CQ4-mutated fibroblasts had a strongly impaired proliferative capacity linked to high senescence rates and a reduction in the proportion of cycling cells, reflecting the involvement of CoQ_{10} in pyrimidine synthesis [2, 5, 7].

A major obstacle to study this disorder is the lack of genotype-phenotype association. Human diseases are generally studied once the full (epi)genetic events (i.e. mutations) are already in place and, therefore, the mechanisms of disease pathophysiology are not amenable to analysis with primary patient samples. Patient-specific iPSC can serve to model human disease since their re-differentiation potential provides a unique strategy to explore the developmental impact of disease-specific mutations on human stem cell fate, especially in early-onset or developmental diseases[27, 47, 48]. We generated and CRISPR/Cas9 corrected iPSC from a patient with a mutation in *COQ4* in an attempt to model CoQ_{10} deficiency by analyzing its impact on MRC/mitochondrial activity and neural and skeletal muscle development. Of note, COQ4-mutated cells were less efficiently reprogrammed, likely reflecting the impaired proliferation of CQ4-F. Nevertheless, undifferentiated CQ4-iPSCs were functionally indistinguishable from Ctrl-iPSCs.

We show for the first time the levels of CoQ_{10} in a panel of pluripotent stem cell lines. Interestingly, cell reprogramming failed to reestablish CoQ_{10} levels/biosynthesis in mutated cells, but this were fully restored upon *COQ4* correction, demonstrating the causal effect of c.483G>C *COQ4* mutation in the metabolic dysfunctional phenotype associated with CoQ_{10} deficiency. This data together with previous data in yeast[20, 49, 50] may highlight the evolutionary conserved role of CoQ_{10} in mitochondrial function by regulating OxPhos and ultimately ATP synthesis. Indeed, MRC complexes I+III and II+III, OxPhos, and glycolysis were all severely impaired in CQ4-iPSC, which required a 2-fold increase in OCR and ECAR to generate the same concentration of ATP. The increased proton leak in CQ4-iPSC represents ATP-independent respiration and

an increase in the passive leak of protons from the inner mitochondrial membrane, linking CoQ_{10} with proton shuttling in pluripotent stem cells[47].

Neurological manifestations are very common in CoQ_{10}-deficient patients[16-18]. Interestingly, our patient failed to exhibit neurological symptoms other than modest mental retardation. Because the impact of *COQ* mutations in neurodevelopment remains unclear, we studied the developmental influence of the *COQ4* mutation in neurogenesis using well-established protocols**.** Our analysis revealed that the c.483 G>C mutation in *COQ4* does not impact DA or MN neurogenesis from iPSCs, thus recapitulating the patient's normal neurological phenotype.

Life-threating rhabdomyolysis was severe in this patient, and eventually led to myoglobinuria and nephrotic toxicity, causing the patient's death. We used a sophisticated differentiation strategy to generate SkM from iPSC, which proceeds through an initial myogenic induction based on the generation of $PAX7^+$ myogenic progenitors, and subsequent myocyte/myotube maturation[32]. Our data clearly show that CQ4-iPSC-differentiated SkM recapitulates CoQ_{10} deficiency-associated SkM functional and metabolic defects. First, CQ4-$PAX7^+$ myogenic progenitors exhibited 1-log reduced cell expansion within a 15-day period, associated with increased levels of senescence, which might likely be due to increased ROS production. These dysfunctional properties were corrected in genome-edited $PAX7^+$ myogenic progenitors. Second, maturation of CQ4-$PAX7^+$ myogenic progenitors was lower than in Ctrl-$PAX7^+$ counterparts. The generation of mature $MYH1^+$ cells and the expression of CK, a master SkM enzyme for the rapid buffering and regeneration of ATP, were decreased significantly. These parameters were recovered in corrected myocytes from $CQ4^{ed}$-$PAX7^+$ cells. Gene expression analysis of mature myogenic mature markers confirmed the functional-metabolic SkM dysfunction associated with CoQ_{10} deficiency, demonstrating the causal link of c.483G>C *COQ4* mutation in the impaired myogenic development and reproducing the main phenotypic manifestation of the disease. Third, mitochondrial morphometric imaging and analysis of MRC activity revealed

abnormalities in mitochondrial morphology and a 50% decrease in the activity of MRC complex I+III, indicating that the *COQ4* mutation negatively impacts the mitochondrial/metabolic function of iPSC-derived SkM derivatives generated from PAX7^{+} myogenic progenitors. These mitochondrial dynamics-associated parameters and MRC complexes activity were restored in CQ4^{ed}-PAX7^{+} iPSC-derived myocytes/myotubes. Thus, genetic correction of *COQ4* mutation rescued the mitochondrial function of *COQ4*-mutated SkM.

In summary, we have established a patient-specific iPSC-based disease model for CoQ_{10} deficiency mediated by a heterozygous mutation in *COQ4*. Our findings provide evidence that the *COQ4* mutation faithfully reproduces all the disease clinical phenotypes including SkM dysfunction, metabolic deficits as well as absence of neurological manifestations. This may assist in the study of complex genotype-phenotype associations observed in CoQ_{10} deficiency, opening avenues for testing new drugs to treat CoQ_{10} deficiency.

METHODS

Methods and any associated reference are available in the online version of the paper

AUTHOR CONTRIBUTION

D.R-M: conceived the study, designed and performed experiments, analyzed data and wrote the manuscript. C.S-O, J.C, G.G, JA.R, V. R-B, C.B, P.G-R, A.G, C.P, A.M-L, A.C, I.V: performed experiments and analyzed data. R.A, P.M-C, J.L-B, P.N: provided biological samples, clinical data and advice. P.M: conceived the study, designed experiments, analyzed data and wrote the manuscript.

ACKNOWLEDGMENTS AND FINANCIAL SUPPORT: This work was supported by the ISCIII/FEDER (E-Rare-2 Call PI12/03112) and the European Research Council (ERC-2014-CoG-646903) to P.M. D.R.M and C.P are supported by PFIS scholarships (FI11/0511 and FI12/00468, respectively). C.B is supported by a Miguel Servet II contract (CPII13/00011). P.M also acknowledges the financial support from The Obra Social La Caixa-Fundació Josep Carreras and The Generalitat de Catalunya (SGR330). P.M and J.L-B are investigators of the Spanish Cell Therapy cooperative network (TERCEL).

CONFLICT OF INTEREST: The authors have no conflict of interest to disclose. All authors have read and approved the manuscript in its present form.

REFERENCES

1. Turunen, M., Olsson, J. & Dallner, G. Metabolism and function of coenzyme Q. *Biochimica et biophysica acta* **1660**, 171-199 (2004).
2. Lopez-Lluch, G., Rodriguez-Aguilera, J.C., Santos-Ocana, C. & Navas, P. Is coenzyme Q a key factor in aging? *Mechanisms of ageing and development* **131**, 225-235 (2010).
3. Desbats, M.A., Lunardi, G., Doimo, M., Trevisson, E. & Salviati, L. Genetic bases and clinical manifestations of coenzyme Q10 (CoQ 10) deficiency. *Journal of inherited metabolic disease* **38**, 145-156 (2015).
4. Salviati, L. *et al.* Infantile encephalomyopathy and nephropathy with CoQ10 deficiency: a CoQ10-responsive condition. *Neurology* **65**, 606-608 (2005).
5. Lopez-Martin, J.M. *et al.* Missense mutation of the COQ2 gene causes defects of bioenergetics and de novo pyrimidine synthesis. *Human molecular genetics* **16**, 1091-1097 (2007).
6. Mollet, J. *et al.* Prenyldiphosphate synthase, subunit 1 (PDSS1) and OH-benzoate polyprenyltransferase (COQ2) mutations in ubiquinone deficiency and oxidative phosphorylation disorders. *The Journal of clinical investigation* **117**, 765-772 (2007).
7. Quinzii, C.M. *et al.* Reactive oxygen species, oxidative stress, and cell death correlate with level of CoQ10 deficiency. *FASEB journal : official publication of the Federation of American Societies for Experimental Biology* **24**, 3733-3743 (2010).
8. Heeringa, S.F. *et al.* COQ6 mutations in human patients produce nephrotic syndrome with sensorineural deafness. *The Journal of clinical investigation* **121**, 2013-2024 (2011).
9. Mollet, J. *et al.* CABC1 gene mutations cause ubiquinone deficiency with cerebellar ataxia and seizures. *American journal of human genetics* **82**, 623-630 (2008).
10. Lagier-Tourenne, C. *et al.* ADCK3, an ancestral kinase, is mutated in a form of recessive ataxia associated with coenzyme Q10 deficiency. *American journal of human genetics* **82**, 661-672 (2008).
11. Ashraf, S. *et al.* ADCK4 mutations promote steroid-resistant nephrotic syndrome through CoQ10 biosynthesis disruption. *The Journal of clinical investigation* **123**, 5179-5189 (2013).
12. Duncan, A.J. *et al.* A nonsense mutation in COQ9 causes autosomal-recessive neonatal-onset primary coenzyme Q10 deficiency: a potentially treatable form of mitochondrial disease. *American journal of human genetics* **84**, 558-566 (2009).
13. Rotig, A. *et al.* Quinone-responsive multiple respiratory-chain dysfunction due to widespread coenzyme Q10 deficiency. *Lancet* **356**, 391-395 (2000).
14. Lopez, L.C. *et al.* Leigh syndrome with nephropathy and CoQ10 deficiency due to decaprenyl diphosphate synthase subunit 2 (PDSS2) mutations. *American journal of human genetics* **79**, 1125-1129 (2006).
15. Freyer, C. *et al.* Rescue of primary ubiquinone deficiency due to a novel COQ7 defect using 2,4-dihydroxybensoic acid. *Journal of medical genetics* **52**, 779-783 (2015).
16. Quinzii, C.M. & Hirano, M. Primary and secondary CoQ(10) deficiencies in humans. *BioFactors* **37**, 361-365 (2011).

17. Artuch, R. *et al.* Cerebellar ataxia with coenzyme Q10 deficiency: diagnosis and follow-up after coenzyme Q10 supplementation. *Journal of the neurological sciences* **246**, 153-158 (2006).
18. Artuch, R., Salviati, L., Jackson, S., Hirano, M. & Navas, P. Coenzyme Q10 deficiencies in neuromuscular diseases. *Advances in experimental medicine and biology* **652**, 117-128 (2009).
19. Trevisson, E., DiMauro, S., Navas, P. & Salviati, L. Coenzyme Q deficiency in muscle. *Current opinion in neurology* **24**, 449-456 (2011).
20. Marbois, B., Gin, P., Gulmezian, M. & Clarke, C.F. The yeast Coq4 polypeptide organizes a mitochondrial protein complex essential for coenzyme Q biosynthesis. *Biochimica et biophysica acta* **1791**, 69-75 (2009).
21. Casarin, A. *et al.* Functional characterization of human COQ4, a gene required for Coenzyme Q10 biosynthesis. *Biochemical and biophysical research communications* **372**, 35-39 (2008).
22. Salviati, L. *et al.* Haploinsufficiency of COQ4 causes coenzyme Q10 deficiency. *Journal of medical genetics* **49**, 187-191 (2012).
23. Brea-Calvo, G. *et al.* COQ4 mutations cause a broad spectrum of mitochondrial disorders associated with CoQ10 deficiency. *American journal of human genetics* **96**, 309-317 (2015).
24. Acosta, M.J. *et al.* Coenzyme Q biosynthesis in health and disease. *Biochimica et biophysica acta* (2016).
25. Montero, R. *et al.* Clinical, biochemical and molecular aspects of cerebellar ataxia and Coenzyme Q10 deficiency. *Cerebellum* **6**, 118-122 (2007).
26. Emmanuele, V. *et al.* Heterogeneity of coenzyme Q10 deficiency: patient study and literature review. *Archives of neurology* **69**, 978-983 (2012).
27. Wu, S.M. & Hochedlinger, K. Harnessing the potential of induced pluripotent stem cells for regenerative medicine. *Nature cell biology* **13**, 497-505 (2011).
28. Gaj, T., Gersbach, C.A. & Barbas, C.F., 3rd ZFN, TALEN, and CRISPR/Cas-based methods for genome engineering. *Trends in biotechnology* **31**, 397-405 (2013).
29. Takahashi, K., Okita, K., Nakagawa, M. & Yamanaka, S. Induction of pluripotent stem cells from fibroblast cultures. *Nature protocols* **2**, 3081-3089 (2007).
30. Bueno, C. *et al.* Reprogramming human B cells into induced pluripotent stem cells and its enhancement by C/EBPalpha. *Leukemia* **30**, 674-682 (2016).
31. Sun, N. *et al.* Feeder-free derivation of induced pluripotent stem cells from adult human adipose stem cells. *Proceedings of the National Academy of Sciences of the United States of America* **106**, 15720-15725 (2009).
32. Darabi, R. *et al.* Human ES- and iPS-derived myogenic progenitors restore DYSTROPHIN and improve contractility upon transplantation in dystrophic mice. *Cell stem cell* **10**, 610-619 (2012).
33. Woods, N.B. *et al.* Brief report: efficient generation of hematopoietic precursors and progenitors from human pluripotent stem cell lines. *Stem cells* **29**, 1158-1164 (2011).
34. Hu, B.Y. *et al.* Neural differentiation of human induced pluripotent stem cells follows developmental principles but with variable potency. *Proceedings of the National Academy of Sciences of the United States of America* **107**, 4335-4340 (2010).
35. Kriks, S. *et al.* Dopamine neurons derived from human ES cells efficiently engraft in animal models of Parkinson's disease. *Nature* **480**, 547-551 (2011).

36. Amoroso, M.W. *et al.* Accelerated high-yield generation of limb-innervating motor neurons from human stem cells. *The Journal of neuroscience : the official journal of the Society for Neuroscience* **33**, 574-586 (2013).
37. Marchetto, M.C. *et al.* Non-cell-autonomous effect of human SOD1 G37R astrocytes on motor neurons derived from human embryonic stem cells. *Cell stem cell* **3**, 649-657 (2008).
38. Burkhardt, M.F. *et al.* A cellular model for sporadic ALS using patient-derived induced pluripotent stem cells. *Molecular and cellular neurosciences* **56**, 355-364 (2013).
39. Koopman, W.J. *et al.* Inhibition of complex I of the electron transport chain causes O2-. -mediated mitochondrial outgrowth. *American journal of physiology. Cell physiology* **288**, C1440-1450 (2005).
40. Yubero, D. *et al.* Molecular diagnosis of coenzyme Q10 deficiency. *Expert review of molecular diagnostics* **15**, 1049-1059 (2015).
41. Quinzii, C.M. & Hirano, M. Coenzyme Q and mitochondrial disease. *Developmental disabilities research reviews* **16**, 183-188 (2010).
42. DiMauro, S. & Schon, E.A. Mitochondrial disorders in the nervous system. *Annual review of neuroscience* **31**, 91-123 (2008).
43. Quinzii, C.M. *et al.* Respiratory chain dysfunction and oxidative stress correlate with severity of primary CoQ10 deficiency. *FASEB journal : official publication of the Federation of American Societies for Experimental Biology* **22**, 1874-1885 (2008).
44. Lopez, L.C. *et al.* Treatment of CoQ(10) deficient fibroblasts with ubiquinone, CoQ analogs, and vitamin C: time- and compound-dependent effects. *PloS one* **5**, e11897 (2010).
45. Montini, G., Malaventura, C. & Salviati, L. Early coenzyme Q10 supplementation in primary coenzyme Q10 deficiency. *The New England journal of medicine* **358**, 2849-2850 (2008).
46. Chung, W.K. *et al.* Mutations in COQ4, an essential component of coenzyme Q biosynthesis, cause lethal neonatal mitochondrial encephalomyopathy. *Journal of medical genetics* **52**, 627-635 (2015).
47. Cooper, O. *et al.* Pharmacological rescue of mitochondrial deficits in iPSC-derived neural cells from patients with familial Parkinson's disease. *Science translational medicine* **4**, 141ra190 (2012).
48. Ramos-Mejia, V., Fraga, M.F. & Menendez, P. iPSCs from cancer cells: challenges and opportunities. *Trends in molecular medicine* **18**, 245-247 (2012).
49. Ozeir, M. *et al.* Coenzyme Q biosynthesis: Coq6 is required for the C5-hydroxylation reaction and substrate analogs rescue Coq6 deficiency. *Chemistry & biology* **18**, 1134-1142 (2011).
50. Cui, T.Z. & Kawamukai, M. Coq10, a mitochondrial coenzyme Q binding protein, is required for proper respiration in Schizosaccharomyces pombe. *The FEBS journal* **276**, 748-759 (2009).

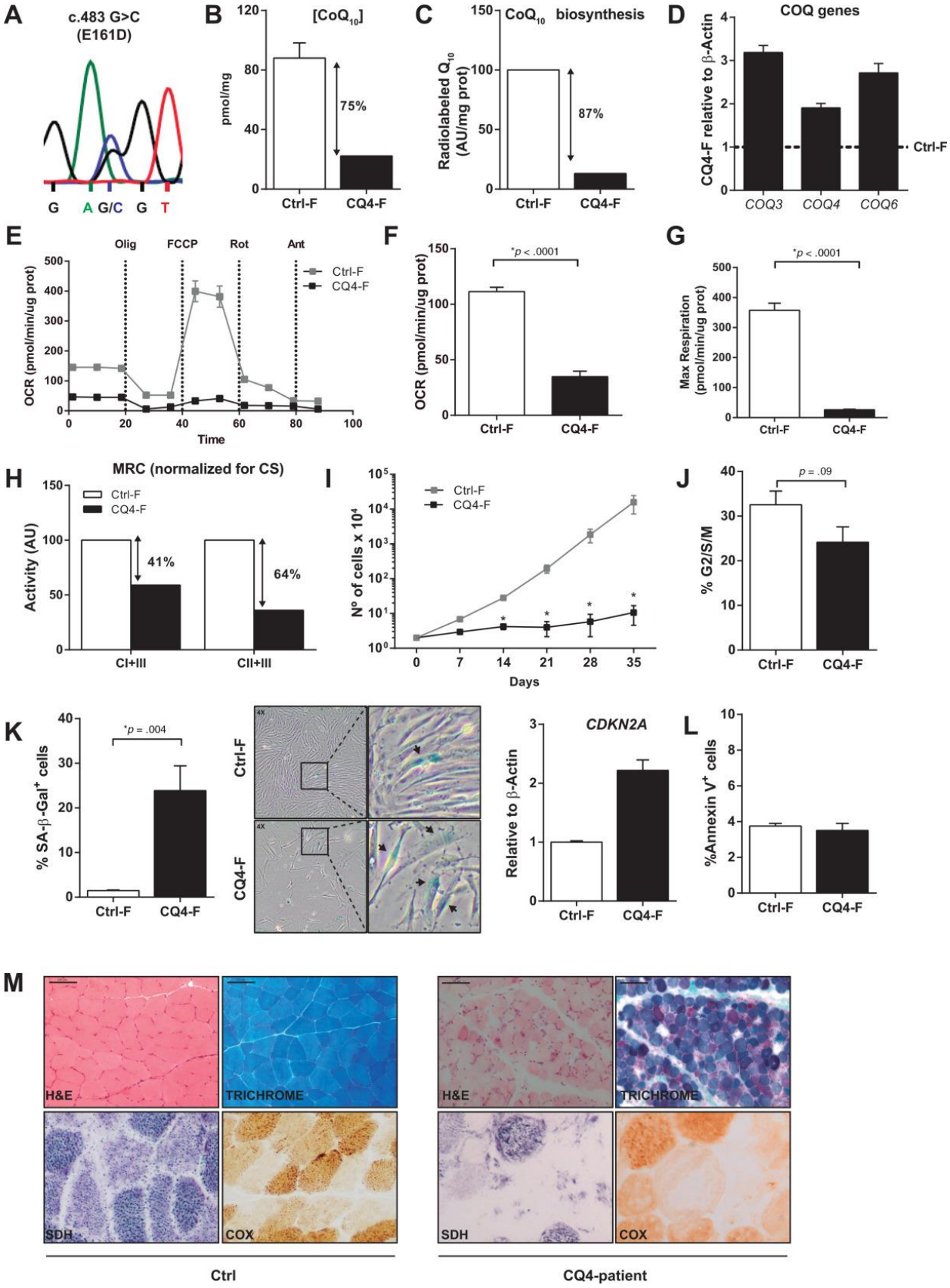
A
c.483 G>C
(E161D)
G A G/C G T
B
[CoQ10]
pmol/mg
75%
Ctrl-F
CQ4-F
C
CoQ10 biosynthesis
Radiolabeled Q10
(AU/mg prot)
87%
D
COQ genes
CQ4-F relative to β-Actin
COQ3
COQ4
COQ6
E
Olig
FCCP
Rot
Ant
OCR (pmol/min/ug prot)
Time
F
*p < .0001
G
Max Respiration
(pmol/min/ug prot)
H
MRC (normalized for CS)
Activity (AU)
41%
64%
CI+III
CII+III
I
Nº of cells x 10⁴
Days
J
p = .09
% G2/S/M
K
*p = .004
% SA-β-Gal+ cells
CDKN2A
Relative to β-Actin
L
%Annexin V+ cells
M
H&E
TRICHROME
SDH
COX
Ctrl
CQ4-patient

Figure 1: Biochemical, metabolic, proliferative and histological characterization of *COQ4*-mutated fibroblasts. (A) Sanger DNA sequencing confirming the heterozygous c.483 G>C mutation in the patient's fibroblasts. **(B)** Seventy-five percent reduction in [CoQ_{10}] in CQ4-F relative to Ctrl-F. **(C)** Eighty-seven percent reduction in CoQ_{10} biosynthesis in CQ4-F relative to Ctrl-F. **(D)** qRT-PCR reflecting a higher expression of *COQ3, COQ4* and *COQ6* genes in CQ4-F than in Ctrl-F. **(E)** Defective MRC complex I+III and II+III activities relative to citrate synthase in CQ4-F. **(F)** Fibroblast proliferation of Ctrl-F and CQ4-F. **(G)** Cell cycle analysis of Ctrl-F and CQ4-F. **(H)** Senescence-associated β-galactosidase quantification of Ctrl-F and CQ4-F and representative image (4×) (*left panel*), and qRT-PCR expression of *p16/CDKN2A* (right panel). **(I)** FACS quantification of apoptotic cells (Annexin V^+). **(J)** Patient's muscle histology revealing mitochondrial alterations after rhabdomyolysis. Values are expressed as mean±SEM. CQ4-F: *COQ4* mutated primary fibroblasts; Ctrl-F: Control primary fibroblasts; H&E: Hematoxylin and eosin; SDH: Succinate dehydrogenase; COX: Cytochrome c oxidase.

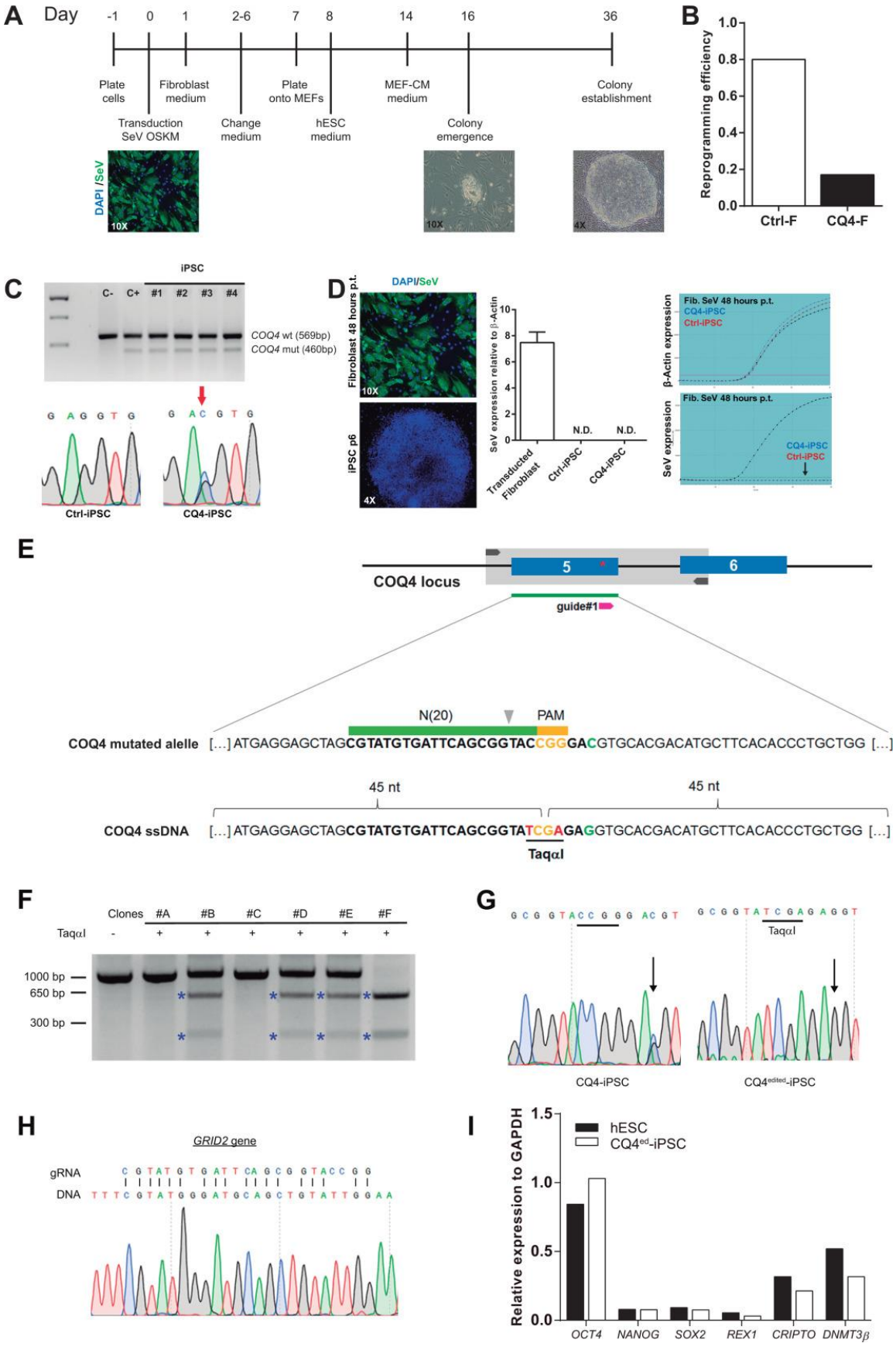
A
Day
-1
0
1
2-6
7
8
14
16
36
Plate cells
Transduction SeV OSKM
Fibroblast medium
Change medium
Plate onto MEFs
hESC medium
MEF-CM medium
Colony emergence
Colony establishment
DAPI/SeV
10X
10X
4X
B
Reprogramming efficiency
1.0
0.8
0.6
0.4
0.2
0.0
Ctrl-F
CQ4-F
C
iPSC
C-
C+
#1
#2
#3
#4
COQ4 wt (569bp)
COQ4 mut (460bp)
G A G G T G
G A C G T G
Ctrl-iPSC
CQ4-iPSC
D
DAPI/SeV
Fibroblast 48 hours p.t.
10X
iPSC p6
4X
SeV expression relative to β-Actin
10
8
6
4
2
0
N.D.
N.D.
Transducted Fibroblast
Ctrl-iPSC
CQ4-iPSC
β-Actin expression
Fib. SeV 48 hours p.t.
CQ4-iPSC
Ctrl-iPSC
SeV expression
Fib. SeV 48 hours p.t.
CQ4-iPSC
Ctrl-iPSC
E
COQ4 locus
5
6
guide#1
N(20)
PAM
COQ4 mutated alelle […] ATGAGGAGCTAGCGTATGTGATTCAGCGGTACCGGGACGTGCACGACATGCTTCACACCCTGCTGG […]
45 nt
45 nt
COQ4 ssDNA […] ATGAGGAGCTAGCGTATGTGATTCAGCGGTATCGAGAGGTGCACGACATGCTTCACACCCTGCTGG […]
TaqαI
F
Clones
#A
#B
#C
#D
#E
#F
TaqαI
-
+
+
+
+
+
+
1000 bp
650 bp
300 bp
G
G C G G T A C C G G G A C G T
G C G G T A T C G A G A G G T
TaqαI
CQ4-iPSC
CQ4edited-iPSC
H
GRID2 gene
gRNA
DNA
C G T A T G T G A T T C A G C G G T A C C G G
T T T C G T A T G G G A T G C A G C T G T A T T G G A A
I
Relative expression to GAPDH
1.5
1.0
0.5
0.0
hESC
CQ4ed-iPSC
OCT4
NANOG
SOX2
REX1
CRIPTO
DNMT3β

Figure 2: Generation of *COQ4*-mutated iPSCs and CRISPR/Cas9-mediated gene edition. (A) Schematic outline of the reprogramming process. **(B)** Reprogramming efficiency for Ctrl-F and CQ4-F. **(C)** PCR and sequencing confirming the presence of *COQ4*-mutated allele in several representative CQ4-iPSC clones. **(D)** Immunostaining confirming high-level infection with SeV 48 h post-transduction and SeV elimination on iPSC at p8-10 (*left panel*). qPCR reflecting complete absence of SeV at p8-10 (*right panel*). **(E)** Schematic overview for the strategy of CRISPR/Cas9 mediated targeting to the *COQ4* locus. Sequence and synonymous modifications in the ssDNA. **(F)** Identification of the edited iPSC clones by Taqα1 allele digestion in the genomic DNA after single cell cloning. **(G)** Sanger DNA sequencing confirming the gene edition. **(H)** Sanger DNA sequencing of the major predicted off-target *GRID2* gene. **(I)** qRT-PCR for the pluripotency genes *OCT4, SOX2, REX1, NANOG, CRIPTO* and *DNMT3β* in hESC and CQ4^{ed}-iPSC. Values are expressed as mean±SEM. CQ4-F: *COQ4* mutated primary fibroblasts; Ctrl-F: Control primary fibroblasts; CQ4-iPSC: *COQ4* mutated iPSC; Ctrl-iPSC: Control iPSC; CQ4^{ed}-iPSC: *COQ4*-edited iPSC.

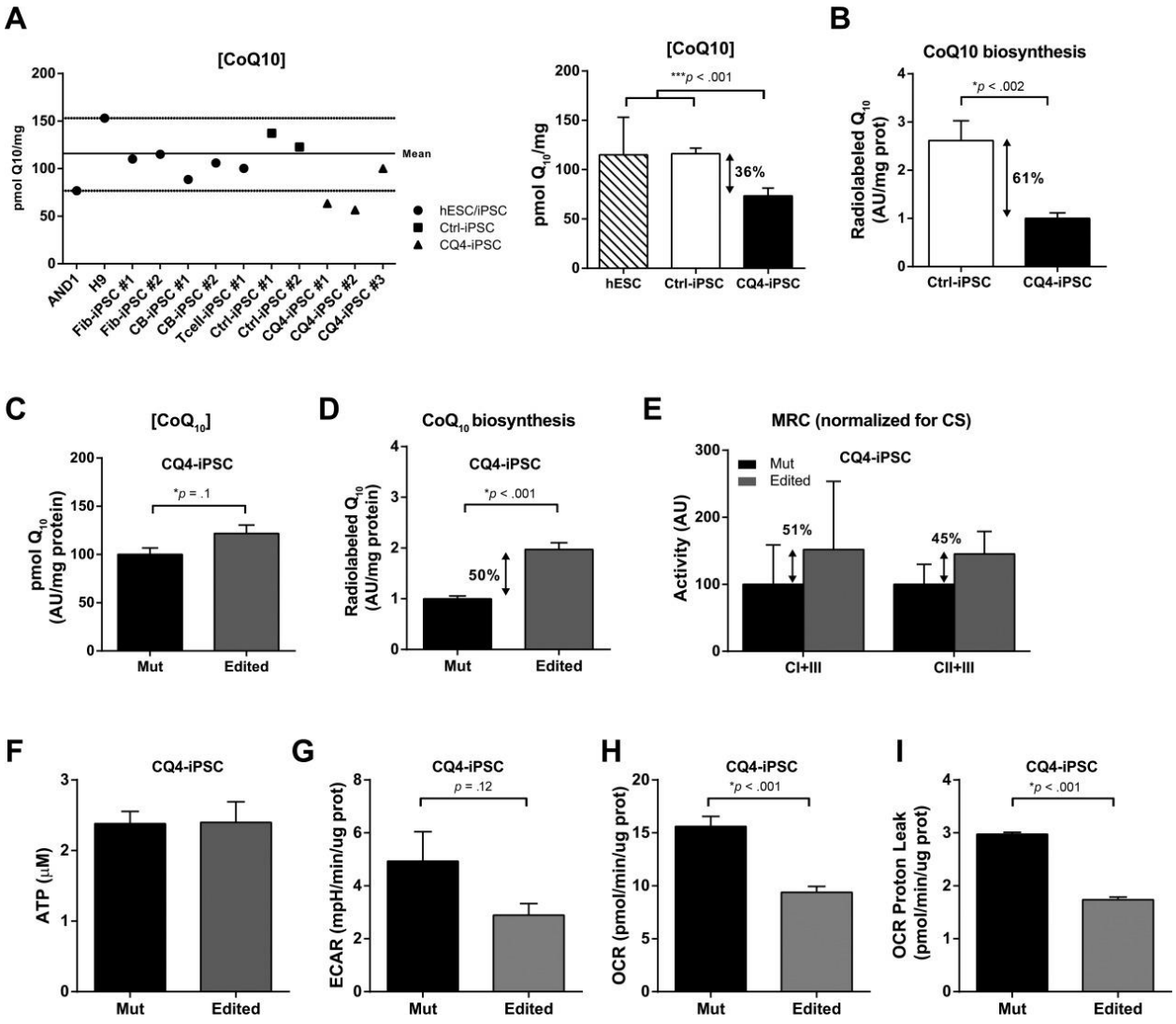

Figure 3: Genome editing of c.483 G>C *COQ4* mutation reverses CoQ_{10} deficiency and metabolic dysfunction retained in CQ4-iPSC. (A) *Left,* concentration of CoQ_{10} in a panel of hESC (H9, AND1), fibroblast-derived iPSC and blood-derived iPSC (●), Ctrl-iPSC (■) and CQ4-iPSC (▲). Solid line represents the mean; dotted lines represent the range. *Right,* summary of [CoQ_{10}] in hESC (n=2), Ctrl-iPSC (n=14) and CQ4-iPSC (n=9). **(B)** Sixty-one percent reduction in CoQ_{10} biosynthesis in CQ4-iPSC (n=9) relative to Ctrl-iPSC (n=14). **(C)** [CoQ_{10}] in mutated and edited CQ4-iPSC. **(D)** CoQ_{10} biosynthesis in mutated and edited CQ4-iPSC. **(E)** MRC complex I+III and II+III activities relative to citrate synthase in mutated and edited CQ4-iPSC. **(F)** [ATP] from mutated (n=6) and edited CQ4-iPSC (n=6). **(G)** Glycolysis-associated extracellular

acidification rate (ECAR) under basal conditions in mutated (n=4) and edited CQ4-iPSC (n=4). **(H)** Oxygen consumption rate (OCR) under basal conditions in mutated (n=6) and edited CQ4-iPSC (n=6). **(I)** OCR proton leak under basal conditions in mutated and edited CQ4-iPSC (n=4). Values are expressed as mean±SEM. Ctrl-iPSC: Control iPSC; CQ4-iPSC: COQ4 mutated iPSC; Fib-iPSC: fibroblast-derived iPSC; CB-iPSC: cord blood-derived iPSC; Tcell-iPSC: T cell-derived iPSC.

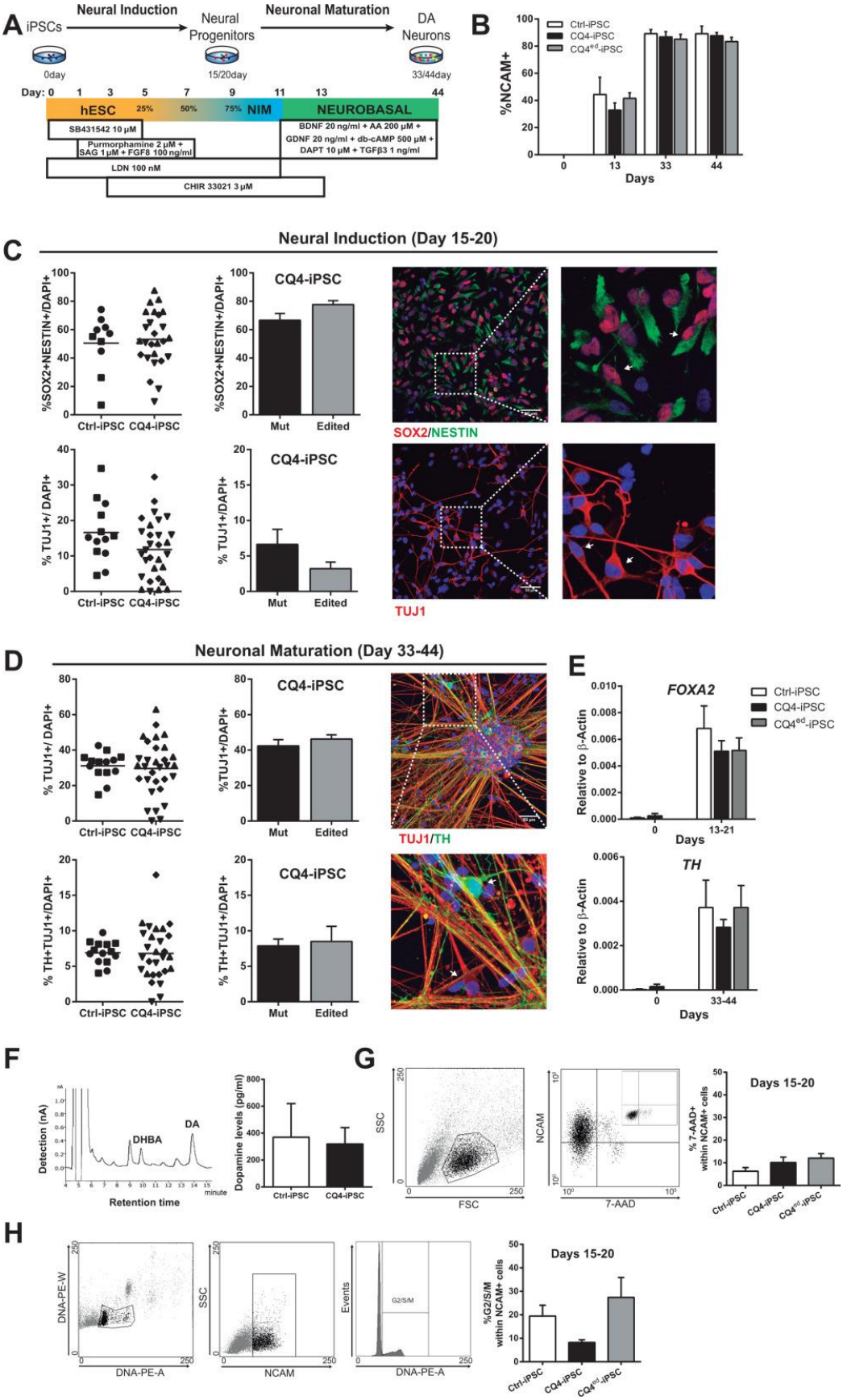
A
iPSCs
Neural Induction
Neural Progenitors
Neuronal Maturation
DA Neurons
0day
15/20day
33/44day
Day: 0 1 3 5 7 9 11 13 44
hESC
25%
50%
75%
NIM
NEUROBASAL
SB431542 10 µM
Purmorphamine 2 µM + SAG 1 µM + FGF8 100 ng/ml
LDN 100 nM
CHIR 33021 3 µM
BDNF 20 ng/ml + AA 200 µM + GDNF 20 ng/ml + db-cAMP 500 µM + DAPT 10 µM + TGFβ3 1 ng/ml
B
Ctrl-iPSC
CQ4-iPSC
CQ4ed-iPSC
%NCAM+
Days
C
Neural Induction (Day 15-20)
%SOX2+NESTIN+/DAPI+
Ctrl-iPSC CQ4-iPSC
CQ4-iPSC
Mut Edited
SOX2/NESTIN
% TUJ1+/ DAPI+
TUJ1
D
Neuronal Maturation (Day 33-44)
TUJ1/TH
% TH+TUJ1+/DAPI+
E
FOXA2
Relative to β-Actin
Days
TH
F
Detection (nA)
DHBA
DA
Retention time
minute
Dopamine levels (pg/ml)
G
SSC
FSC
NCAM
7-AAD
Days 15-20
% 7-AAD+ within NCAM+ cells
H
DNA-PE-W
DNA-PE-A
NCAM
Events
G2/S/M
%G2/S/M within NCAM+ cells

Figure 4: Dopaminergic (DA) differentiation of Ctrl-iPSC, CQ4-iPSC and CQ4-edited iPSC. (A) *Top,* scheme of neuronal differentiation depicting two stages: neural induction (up to day 15–20) and neuronal maturation (up to day 33–44). *Bottom*, detailed differentiation protocol used. **(B)** Flow cytometry quantification of $NCAM^+$ cells throughout DA differentiation. **(C)** Analysis of $SOX2^+NESTIN^+$ neural progenitors (*top panels*, N=42) and $TUJ1^+$ neurons (*bottom panels,* N=49). *Left*, differentiation efficiency in Ctrl-iPSC and CQ4-iPSC at day 15–20 of iPSC differentiation. *Middle*, DA differentiation efficiency in mutated and edited CQ4-iPSC. *Right,* representative images of immunostaining (40×) and magnification for $SOX2^+NESTIN^+$ and $TUJ1^+$ cells. White arrows point to positive cells. Scale bar, 50 μm. **(D)** Analysis of the $TUJ1^+$ neurons (*top panels*, N=51) and TH^+TUJ1^+ DA (*bottom panels,* N=48). *Left*, differentiation efficiency in Ctrl-iPSC and CQ4-iPSC at day 33–44 of iPSC development. *Middle*, DA differentiation efficiency in mutated and edited CQ4-iPSC. *Right,* representative image of immunostaining (40×) and magnification for $TUJ1^+$ and $TUJ1^+TH^+$ cells. White arrows point to positive cells. Scale bar, 50 μm. **(E)** Expression of the midbrain precursor-specific gene *FOXA2* after 15–20 days and the DA-specific gene *TH* after 33–44 days in differentiating Ctrl-, CQ4- and $CQ4^{ed}$- iPSC cultures. **(F)** Representative HPLC chromatogram (*left)* and levels (*right*) of dopamine release *in vitro* from differentiating Ctrl-, CQ4- and $CQ4^{ed}$- iPSC cultures. **(G)** FACS quantification of dead cells (7-AAD+) within the $NCAM^+$ neural population at day 15–20 of iPSC differentiation. **(H)** Cell cycle analysis (G2/S/M) within the $NCAM^+$ population at day 15–20 of iPSC differentiation. Data are presented as mean±SEM.

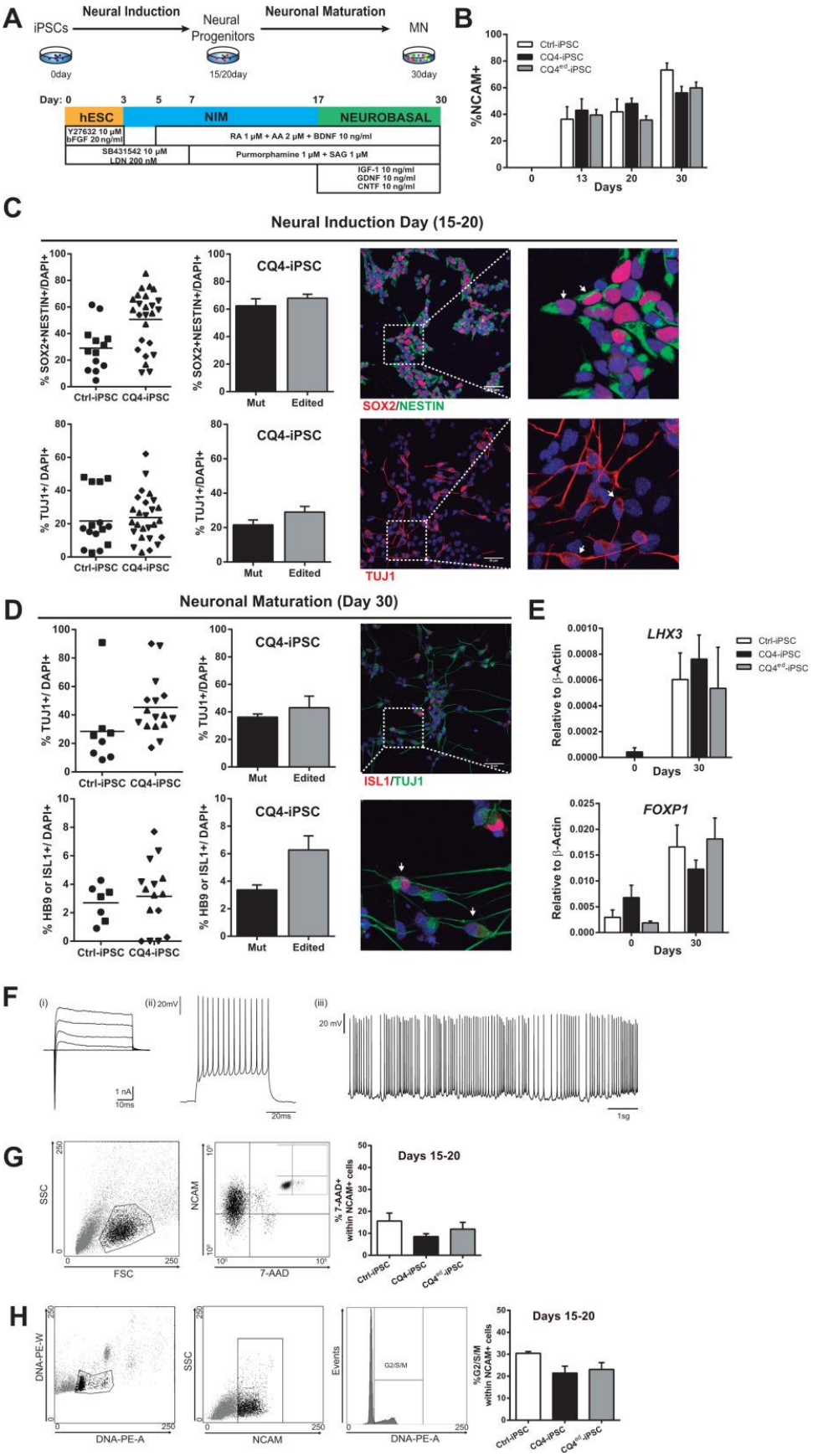
A
Neural Induction
iPSCs
Neural Progenitors
Neuronal Maturation
MN
0day
15/20day
30day
Day: 0 3 5 7 17 30
hESC
NIM
NEUROBASAL
Y27632 10 µM bFGF 20 ng/ml
RA 1 µM + AA 2 µM + BDNF 10 ng/ml
SB431542 10 µM LDN 200 nM
Purmorphamine 1 µM + SAG 1 µM
IGF-1 10 ng/ml GDNF 10 ng/ml CNTF 10 ng/ml
B
Ctrl-iPSC
CQ4-iPSC
CQ4ed-iPSC
%NCAM+
Days
C
Neural Induction Day (15-20)
% SOX2+NESTIN+/DAPI+
Ctrl-iPSC CQ4-iPSC
CQ4-iPSC
Mut Edited
SOX2/NESTIN
% TUJ1+/ DAPI+
TUJ1
D
Neuronal Maturation (Day 30)
% TUJ1+/ DAPI+
ISL1/TUJ1
% HB9 or ISL1+/ DAPI+
E
LHX3
FOXP1
Relative to β-Actin
Days
F
(i)
(ii) 20mV
(iii)
20 mV
1 nA
10ms
20ms
1sg
G
SSC
FSC
NCAM
7-AAD
Days 15-20
% 7-AAD+ within NCAM+ cells
H
DNA-PE-W
DNA-PE-A
SSC
NCAM
Events
G2/S/M
%G2/S/M within NCAM+ cells

Figure 5: Motor neuron (MN) differentiation from Ctrl-iPSC, CQ4-iPSC and CQ4-edited iPSC. (A) *Top,* scheme of neuronal differentiation depicting two stages: neural induction (up to day 15–20) and neuronal maturation (up to day 30). *Bottom*, detailed differentiation protocol used. **(B)** Flow cytometry quantification of $NCAM^+$ cells throughout MN differentiation. **(C)** Analysis of the $SOX2^+NESTIN2^+$ neural progenitors (*top panels*, N=43) and $TUJ1^+$ neurons (*bottom panels,* N=46). *Left*, differentiation efficiency in Ctrl-iPSC and CQ4-iPSC at day 15–20 of iPSC differentiation. *Middle*, MN differentiation efficiency in mutated and edited CQ4-iPSC. *Right*, representative images of immunostaining (40×) and magnification for $SOX2^+NESTIN^+$ and $TUJ1^+$ cells. White arrows point to positive cells. Scale bar, 50 µm. **(D)** Analysis of the $TUJ1^+$ neurons (*top panels*, N=26) and $HB9^+$ or $ISL1^+$ MN (*bottom panels*, N=21). *Left*, differentiation efficiency in Ctrl-iPSC and CQ4-iPSC at day 30 of iPSC development. *Middle*, MN differentiation efficiency in mutated and edited CQ4-iPSC. *Right,* representative images of immunostaining (40×) and magnification for $TUJ1^+$ and $TUJ1^+ISL1^+$. White arrows point to positive cells. Scale bar, 50 µm. **(E)** Expression of MN-specific genes *LHX3* and *FOXP1* after 30 days in differentiating Ctrl-, CQ4- and $CQ4^{ed}$-iPSC cultures. **(F)** Representative electrophysiological analysis of MNs differentiated from CQ4-iPSC. GFP+ MNs were recorded 4–7 days after transfection with a HB9 promoter-GFP reporter. (i) voltage-dependent K^+ and Na^+ currents recorded at various membrane potentials. The holding potential was -70 mV; (ii) Current-clamp recording of action potentials evoked by current injection; (iii) Spontaneous action potentials in MNs recorded in the whole-cell current-clamp configuration. **(G)** FACS quantification of dead cells (7-AAD+) within the $NCAM^+$ neural population at day 15–20 of iPSC differentiation. **(H)** Cell cycle analysis (G2/S/M) within the NCAM+ population at day 15–20 of iPSC differentiation. Data are presented as mean ±SEM.

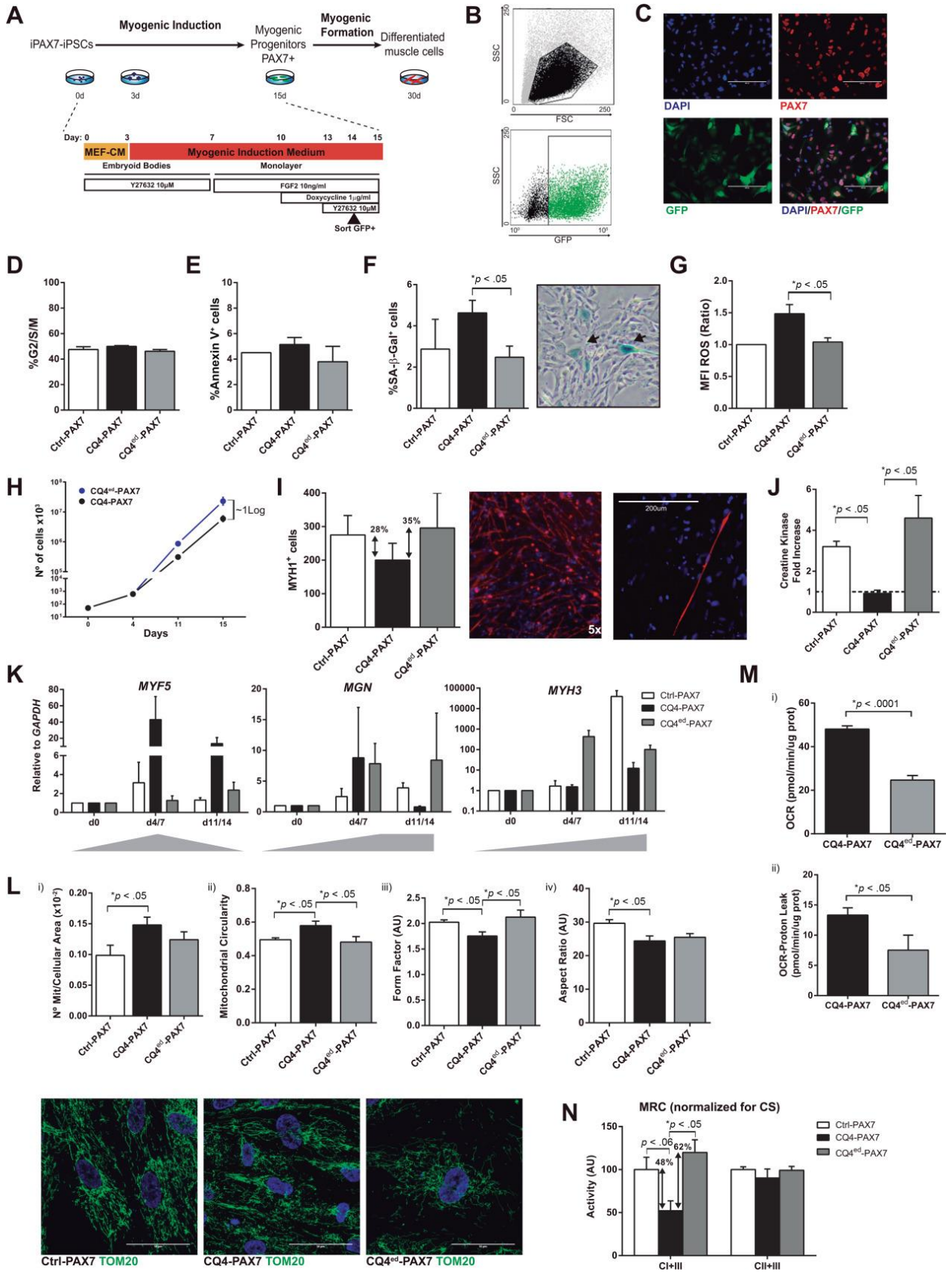
A
Myogenic Induction
iPAX7-iPSCs
Myogenic Progenitors PAX7+
Myogenic Formation
Differentiated muscle cells
0d
3d
15d
30d
Day: 0 3 7 10 13 14 15
MEF-CM
Myogenic Induction Medium
Embryoid Bodies
Monolayer
Y27632 10μM
FGF2 10ng/ml
Doxycycline 1μg/ml
Y27632 10μM
Sort GFP+
B
SSC
FSC
GFP
C
DAPI
PAX7
GFP
DAPI/PAX7/GFP
D
%G2/S/M
E
%Annexin V+ cells
F
%SA-β-Gal+ cells
*p < .05
G
MFI ROS (Ratio)
*p < .05
Ctrl-PAX7
CQ4-PAX7
CQ4ed-PAX7
H
CQ4ed-PAX7
CQ4-PAX7
~1Log
Nº of cells x10³
Days
I
MYH1+ cells
28%
35%
5x
200um
J
Creatine Kinase Fold Increase
*p < .05
*p < .05
K
MYF5
MGN
MYH3
Relative to GAPDH
Ctrl-PAX7
CQ4-PAX7
CQ4ed-PAX7
d0
d4/7
d11/14
M
i)
OCR (pmol/min/ug prot)
*p < .0001
CQ4-PAX7
CQ4ed-PAX7
ii)
OCR-Proton Leak (pmol/min/ug prot)
*p < .05
L
i)
Nº Mit/Cellular Area (x10⁻²)
*p < .05
ii)
Mitochondrial Circularity
*p < .05
*p < .05
iii)
Form Factor (AU)
*p < .05
*p < .05
iv)
Aspect Ratio (AU)
*p < .05
Ctrl-PAX7 TOM20
CQ4-PAX7 TOM20
CQ4ed-PAX7 TOM20
N
MRC (normalized for CS)
Activity (AU)
*p < .05
p < .06
48%
62%
Ctrl-PAX7
CQ4-PAX7
CQ4ed-PAX7
CI+III
CII+III

Figure 6: Impaired skeletal muscle differentiation of CQ4-iPSC is restored upon COQ4 gene editing. **(A)** *Top,* scheme of myogenic differentiation depicting two stages: myogenic induction (up to day 15) and myotubes formation from PAX7^{+} myogenic progenitors (up to day 30). *Bottom*, detailed differentiation protocol used for myogenic induction. **(B)** Representative FACS profile showing PAX7-GFP reporter expression in dox-treated iPSCs. **(C)** Immunostaining (20×) for PAX7^{+}GFP^{+} FACS-purified myogenic progenitors. Scale bar, 200 µm. **(D)** FACS quantification of cycling cells (G2/S/M). **(E)** FACS quantification of apoptotic cells (Annexin V^{+}). **(F)** Senescence-associated β-galactosidase quantification of myogenic derivatives, and representative image (4×). Black arrowheads point to β-gal-positive cells. **(G)** Determination of ROS levels by flow cytometry. **(H)** Expansion of PAX7^{+} myogenic progenitors. **(I)** *Left*, analysis of MYH1^{+} myotubes differentiation in Ctrl-, CQ4- and CQ4^{ed}- PAX7 cultures. *Right,* representative image of MYH1^{+} immunostaining (20×). Scale bar, 200 µm. **(J)** Creatine kinase fold-increase between day 0 and day 11 of differentiation in Ctrl-, CQ4- and CQ4^{ed}- PAX7 myogenic cells (n=6). **(K)** Expression of the SkM-specific genes *MYF5, MGN* and *MYH3* throughout myogenic maturation. Values are expressed as mean±SEM; *p<0.05. The shadow below the graph indicates the temporal expression pattern for each gene during myogenesis. **(L)** *Top,* mitochondrial dynamics for myogenic cells: (i) number of mitochondria/cellular area; (ii) mitochondrial circularity ($4\pi \cdot area/perimeter^2$); (iii) Form Factor (Degree of mitochondrial branching); and (iv) Aspect Ratio (mitochondrial length). *Bottom,* representative images of Ctrl-, CQ4- and CQ4^{ed}- PAX7 myogenic cells stained with TOM20. **(M)** MRC complex I+III and II+III activities relative to citrate synthase in Ctrl-, CQ4- and CQ4^{ed}- PAX7 myogenic cells (n=3). Data are presented as mean ±SEM.